Solution-Processable Exfoliated Zeolite Nanosheets Purified by Density Gradient Centrifugation

Kumar Varoon Agrawal, Berna Topuz, Zheyu Jiang, Kevin Nguenkam, Bahman Elyassi, Lorraine F. Francis, and Michael Tsapatsis
Dept. of Chemical Engineering and Materials Science, University of Minnesota, 151 Amundson Hall, 421 Washington Ave SE, Minneapolis, MN 55455

Marta Navarro
Universidad de Zaragoza, Dept. of Chemical and Environmental Engineering and Instituto de Nanociencia de Aragón (INA), 50018 Zaragoza, Spain

DOI 10.1002/aic.14099
Published online May 1, 2013 in Wiley Online Library (wileyonlinelibrary.com)

Highly crystalline exfoliated MFI-nanosheets can pave the way for large-scale deployment of sub-500-nm zeolite membranes due to their processing and packing advantages. Exfoliated MFI-nanosheets prepared by melt compounding contain a large amount of polymer and unexfoliated particles which are detrimental to the fabrication of ultrathin zeolite membranes. Complete removal of polystyrene from the nanosheet suspension in toluene is demonstrated by centrifugation of the suspension across chlorobenzene as confirmed by thermogravimetric analysis (TGA) data and transmission electron microscopy (TEM) images. Rate-zonal centrifugation in a nonlinear density gradient fractionated exfoliated MFI-nanosheets from unexfoliated particles. The purified nanosheets were highly crystalline as indicated by high-resolution TEM (HRTEM) and electron diffraction (ED). Coating of purified MFI-nanosheets on a smooth α-alumina support, fabricated by filtration of α-alumina suspension, led to a compact, b-oriented, 80-nm-thick film. A mild hydrothermal treatment of the film led to a 200-nm-thick membrane, which demonstrated molecular sieving properties. © 2013 American Institute of Chemical Engineers *AIChE J*, 59: 3458-3467, 2013

Keywords: zeolite nanosheets, density gradient centrifugation, zeolite membrane, membrane support

Introduction

The development of better separation processes was and remains today a major activity for chemical engineers.[1] Among advancements in nanotechnology, thin film fabrication of microporous materials emerged in the last 2 decades as a possible route to high-throughput membranes. Sub-500 nm-thick zeolite films are desirable for large-scale deployment of this technology.[2] These ultrathin zeolite membranes can be fabricated by oriented assembly of high-aspect-ratio zeolite nanosheets on porous supports.[3–5] In contrast to isotropic zeolite nanocrystals, zeolite nanosheets are flexible, allowing them to conform to the rough surface of the underlying support, without the need of support pore masking,[6] or support modification using mesoporous top-layers.[7] Recently, starting from multilamellar MFI,[8] 1.5 unit cell-thick MFI-nanosheets were obtained via exfoliation of the lamella by melt compounding with polystyrene.[4] Dissolution of the polymer-zeolite nanocomposite in toluene, followed by removal of unexfoliated particles by a one-step centrifugation process, yielded structurally and morphologically intact zeolite nanosheets. A simple filtration technique followed by a mild hydrothermal treatment was used to fabricate about 350 nm thick zeolite membranes, which separated *p*-xylene from *o*-xylene.

To fabricate thinner zeolite membranes using these MFI-nanosheets, the coating suspension must be further purified to obtain uniform (in thickness and lateral size) nanosheets, while removing the larger unexfoliated particles and the polystyrene used in the melt compounding process. Polystyrene removal by heat treatment leads to curling and agglomeration of nanosheets, deteriorating their ability to pack and orient in a thin film.[4] Therefore, a method is required to purify nanosheets without inducing structural and morphological damages. Solution processing of nanosheets by density gradient centrifugation (DGC) is one such technique.

In DGC, particles are separated by exploiting the differences in their sedimentation velocity. This is attained by centrifugation of the particles in a fluid medium with density gradient along the depth of the fluid.[9] The density gradient can be linear (linear increase in density along the depth of the fluid), or nonlinear (by stacking of fluids with dissimilar densities). If centrifugation is carried out for a long enough time to achieve equilibrium, particles with identical density accumulate in corresponding density zones along the depth of the fluid (isopycnic sedimentation). In the case of particles with different size and shape but identical density, a non-equilibrium approach is adopted (rate-zonal centrifugation[10]).

Correspondence concerning this article should be addressed to M. Tsapatsis at tsapatsis@umn.edu.

In this case, segregation of particles is time-dependent as, for example, larger particles sediment at a faster rate as compared to the smaller particles.

DGC was first reported as a tool to calculate the molecular weight and partial specific volume of DNA and viruses by isopycnic sedimentation.[11] Leif and Vinograd applied this technique to purify subpopulations of human erythrocytes in a linear density gradient of bovine serum albumin.[12] Since then, density gradient has been used to separate a variety of cells[13–15] and cell fractionates.[16–19] This concept was also applied in measurement of the density of polymeric nanoparticles,[20] as well as their purification[21–23] by isopycnic sedimentation. For example, three different styrene-butyl methacrylate latex particles were fractioned in linear density gradient created by sucrose solution in water, enabling a study of monomer distribution in each type of latex particle.[22]

Recently, density gradient centrifugation has been used to purify carbon nanotubes (CNTs) based on their diameter,[24–28] wall thickness,[29,30] length[31] and aggregation,[32,33] leading to fabrication of next generation thin-film electrical devices. Arnold et al. pioneered isopycnic segregation of nanotubes by surfactant encapsulation of single-wall carbon nanotubes (SWCNTs), leading to change in the density of nanotubes as a function of diameter.[24] A repeated isopycnic ultracentrifugation in a linear density gradient of iodixanol successfully fractionated SWNTs of different diameters. Using a similar principle, double wall CNTs were separated from single and multiwall CNTs, carbonaceous impurities and metallic catalyst particles, for applications in field-effect transistors and transparent conductors.[29] Ghosh et al. applied a nonlinear density gradient to separate highly polydisperse sample of SWCNTs in a single step.[26] Fractionation of CNTs based on their length was reported by nonequilibrium rate-zonal centrifugation by exploiting the transient motion of SWNTS in a dense fluid medium.[31]

DGC has been also applied to purify a variety of spherical nanoparticles. FeCo nanocrystals coated with graphitic shells were separated by nonlinear density gradient.[34] Gold core/silica shell nanoparticles for application in plasmonics nanoantennas were purified using high viscosity iodixanol density gradient.[35] Monodisperse Si nanocrystals were obtained by fractionation in density gradient of 40% 2-4-6 tribromotoluene in cholorobenzene.[36]

Reports of fractionation of particles with sheet-like morphology have been limited. Exfoliated graphene sheets were purified using similar principles applied in fractionation of CNTs in iodixanol density gradient.[37] Sun et al. used rate zonal centrifugation in sucrose density gradient to separate chemically modified graphene in minutes of using ultracentrifugation.[38] Reports of purification of clay particles have been limited to soil mineralogy. DGC in a mixture of tetrabromoethane and acetone was used to identify and separate clay particles saturated by H^+, Ca^{+2}, K^+ and Cs^{+2} ions.[39] Similar density gradient technique was used to fractionate <0.2 μm clay materials from three soils with different Fe-oxide minerology.[40]

Barring a few,[36,40–42] most of the DGC experiments[9–35,37–39] have used aqueous density gradient (iodixanol, sucrose, etc.) for fractionation of particles. However, MFI-nanosheets are difficult to stabilize in aqueous suspensions due to presence of long hydrophobic surfactant embedded in their structure.[8,43,44] Most of the isopycnic fractionations reported in the literature were carried out for a long time (up to a day) using ultracentrifuges, which also puts restriction on the processable volume. Here, we report purification of MFI-nanosheets from polystyrene, organic contaminations, and unexfoliated particles by using rate-zonal centrifugation in nonlinear density gradients created with organic solvents in a regular centrifuge. Fabrication of an ultrathin zeolite membrane on a porous alumina support is demonstrated using the MFI-nanosheets purified by DGC.

Experimental

Purification of nanosheets to remove polystyrene

Nanocomposite of MFI-nanosheets and polystyrene were prepared as reported before.[4] Briefly, multilamellar MFI, prepared by the procedure reported by Ryoo and coworkers,[8] was exfoliated by melt compounding with polystyrene.[45] 3.0 g of exfoliated nanocomposite was dispersed in toluene to yield 1.0% w/w suspension by sonication in a bath sonicator (Branson 5510R-DTH, 135 watts) for 30 min. The resulting suspension was centrifuged (Beckman Coulter, Avanti J-20 XP equipped with JA25.50 rotor) in four 50 mL FEP centrifuge tubes at 40,000 g for 3 h to sediment zeolite nanosheets at the bottom of the centrifuge tubes. Sedimented nanosheets were separated from the supernatant and redispersed in toluene. The centrifugation and re-dispersion process was repeated twice. The resulting nanosheet sediment was then dispersed in 20 mL toluene, and placed on top of 20 mL chlorobenzene in a 50 mL FEP centrifuge tube, drop by drop by a transfer pipette, to create a nonlinear one step density gradient. Centrifugation was carried out at 40,000 g for 3 h. At the end of centrifugation, the nanosheets sedimented at the bottom of the centrifuge tube were collected by pouring out the supernatant. A part of the nanosheet sediment was analyzed by thermogravimetric analysis (TGA) to confirm the removal of polystyrene.

Purification of nanosheets to remove unexfoliated zeolites

The zeolite sediment obtained after removal of polystyrene was dispersed in 20 mL n-octanol by horn sonication (Qsonica Q500, 500 watts, 0.125″ microtip operating at 20% of maximum amplitude) for 3 min followed by sonication in the bath sonicator for 30 min. A nonlinear multilayered density gradient was created in a 50 mL FEP centrifuge tube by sequentially placing 5 mL chloroform ($\rho = 1.48$ g/cc), 5 mL dichloromethane ($\rho = 1.33$ g/cc), 10 mL chlorobenzene ($\rho = 1.10$ g/cc), and finally 20 mL nanosheet suspension in octanol. After centrifugation at 12,000 g for 30 min, the liquid fractions marked by the solvent interfaces were collected by transfer pipettes in separate vials. These fractions were characterized by transmission electron microscopy (TEM). The top fraction (*n*-octanol) was diluted to 40 mL and centrifuged at 40,000 g for 3 h to sediment the purified nanosheets. The sedimented nanosheets were dispersed in 40 mL *n*-octanol by the horn sonication for 3 min followed by sonication in the bath sonicator for 60 min. This suspension was characterized by TEM and high-resolution TEM (HRTEM), and used for fabrication of nanosheet films.

Fabrication of support, thin nanosheet film and membrane

Fabrication of the round α-alumina disks (22 mm in diameter and 3 mm in thickness) by hydraulic pressing of dry

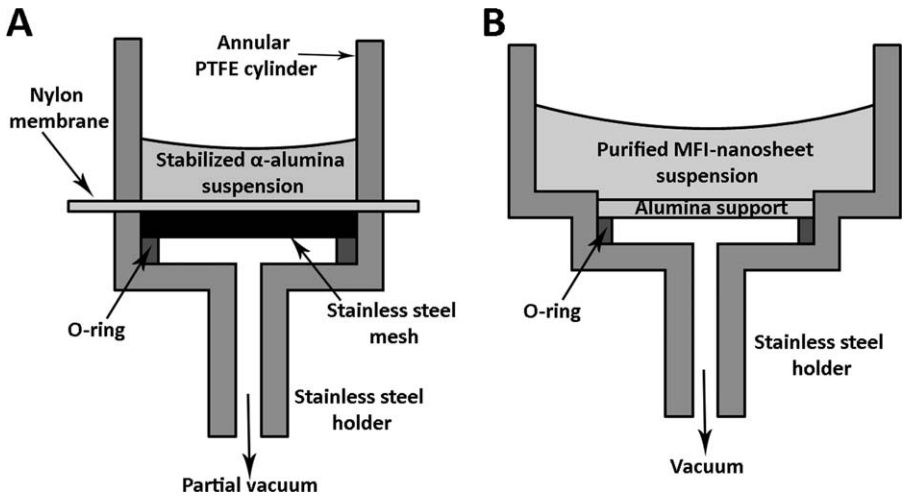

Figure 1. Schematic diagrams showing the experimental setups.

(A) Fabrication of α-alumina support by colloidal processing, and (B) Fabrication of a thin MFI-nanosheet film on the α-alumina support.

α-Al_2O_3 powder (CR-6, Baikowski, average particle size of 400 nm) was carried out as reported before.[46] Supports were sintered at 1160°C for 6 h for mechanical strength.

For fabrication of supports by colloidal processing, α-Al_2O_3 powder was added to water to make a 20 vol % suspension. The suspension was electrostatically stabilized at pH 2.2 by slow addition of HNO_3. Horn sonication for 3 min followed by bath sonication for 90 min was carried out to disperse the agglomerated particles. This suspension was filtered through a 1 μm stainless steel mesh (TWP, Inc., part # MIC1TL5) to remove any remaining large agglomerates. The bubbles in the suspension were suppressed by addition of 3 μL n-octanol/g to the suspension, followed by degassing of the suspension in the bath sonicator. For gypsum mold casting, the alumina suspension was poured inside an annular PTFE cylinder (I.D. = 22 mm) standing vertically on a 25 μm cellulose fiber filter (Whatman) on the gypsum mold. Fabrication of support by filtration was achieved by pouring the alumina suspension inside the annular PTFE cylinder standing vertically on a 0.2 μm nylon membrane (Whatman) under partial vacuum (−14 kPa), as shown in Figure 1A. After 2 h, alumina compacts were removed from the PTFE annulus and dried overnight at room temperature. The surface of each compact was cleaned from the loose alumina particles by blowing it with pressurized nitrogen (80 psig). The compacts were then sintered under air flow (150 mL/min) at 1050°C or 1150°C for 3 h with a heating rate of 2°C/min. To improve the interaction between the support and the zeolite film, the supports were treated with air plasma (Harrick plasma cleaner, PDC-32G) for 2 min before the fabrication of nanosheet film.

Thin nanosheet film was fabricated on alumina supports by vacuum assisted filtration. 0.3 g of nanosheet suspension was diluted with 3.0 g n-octanol and sonicated in the bath sonicator. The sonicated nanosheet suspension was poured over the alumina support held in vacuum in a homemade setup (Figure 1B). At the end of filtration, the disk was dried at 150°C for 4 h, and calcined under air flow (150 mL/min) at 550°C for 6 h with a heating rate of 1°C/min, to remove the organic structure-directing agent (OSDA) from the nanosheet framework. The calcination was carried out in a quartz Petri dish (Technical Glass Products) covered with a cap with a gas inlet and outlet. The retention time of air in the Petri dish was about 2 min.

The growth suspension used to reduce the interparticle gaps in the nanosheet film was prepared as reported before.[4] Briefly, a synthesis sol (60 SiO_2:9 TPAOH: 8100 H_2O: 240 EtOH) was hydrolyzed overnight, and aged at 100°C for 6 h in a Teflon-lined stainless steel autoclave. The alumina disk coated with MFI-nanosheet was placed vertically in the aged synthesis sol, and heated at 100°C for 16 h in a Teflon-lined stainless steel autoclave. The resulting membrane was then calcined under air flow (150 mL/min) in the quartz Petri dish at 480°C for 4 h with heating rate of 0.5°C/min, to remove TPAOH from the membrane framework.

Characterization

TGA analysis (PerkinElmer TGA-7 analyzer) was done to estimate the amount of organic content in the zeolite sediment obtained after purification by DGC in toluene-chlorobenzene gradient. Analysis was carried out by heating a few mg of the zeolite sediment in air flow (100 mL/min) from 130 to 550°C (heating rate of 1°C/min) and maintaining the sample at 550°C for 8 h.

TEM specimens were prepared by depositing a drop of the suspensions on a TEM grid (ultrathin carbon film on holey carbon support film, 400 mesh Cu, Ted Pella) followed by drying the coated grid in ambient conditions. All TEM and high-resolution TEM (HRTEM) studies were conducted using an FEI Tecnai T12 TEM operating at 120 kV and an FEI Tecnai G2 F30 TEM operating at 300 kV, respectively. The images were acquired using a CCD camera.

For preparation of atomic force microscopy (AFM) specimen, 20 μL of purified nanosheet suspension was deposited on a hydrophobic silicon wafer by spin coating at 3000 rpm for 4 min. The nanosheet coating was calcined in air flow at 540°C for 6 h to remove the OSDA from the pores and surface of the nanosheets. AFM was carried out in tapping mode in the repulsive regime using a Molecular Imaging PicoPlus scanning probe microscope (since renamed Agilent 5500 AFM/SPM system). The AFM image analysis was performed using Gwiddion 2.30 software. For calibration of the AFM height data, 2.0 nm steps of the muscovite mica, created by etching a freshly cleaved muscovite mica in 50%

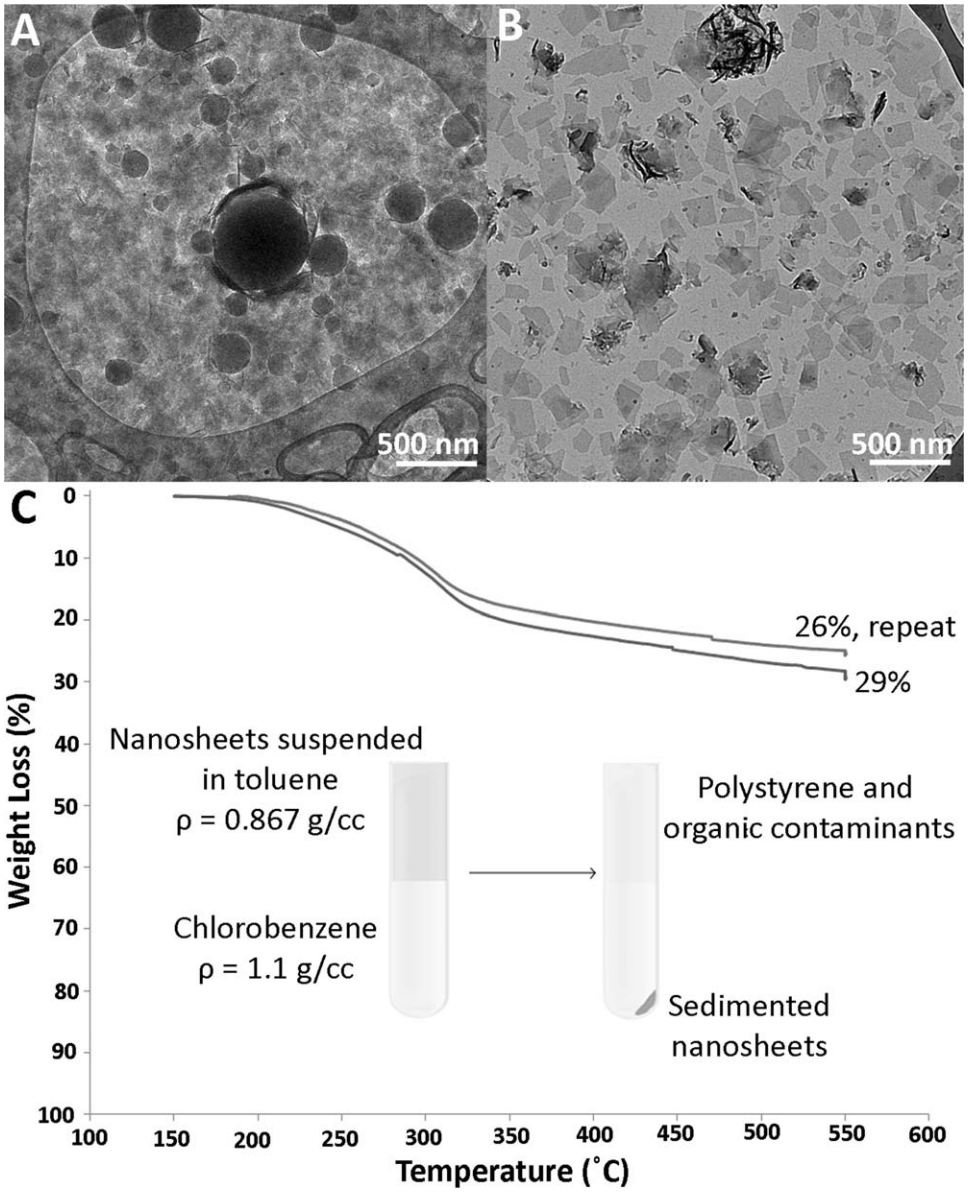

Figure 2. (A) TEM image of MFI-nanosheets sediment before purification by density gradient centrifugation (DGC). The sediment was prepared by 5 cycles of washing in centrifugation and redispersion in toluene. The spheres in the image are polystyrene, which precipitated upon dispersion of the sediment in *n*-octanol, (B) TEM image of MFI-nanosheets purified from polystyrene by nonlinear DGC, and (C) TGA curves from two separate DGC purification experiments showing expected weight loss of nanosheet sediments due to elimination of organic structure directing agent (OSDA).

The schematic below the TGA curves illustrates the experiments for separation of polystyrene from MFI-nanosheets in the toluene-chlorobenzene density gradient.

hydrofluoric acid for 4 h,[47] was used as the calibration standard.

For preparation of cross sections, the nanosheet film and the membrane were coated with approximately 300 nm Au by a sputter coater to protect the surface from beam damages from the focused ion beam (FIB). The cross section was prepared by a FIB equipped with a Ga ion source operating at 30 kV (Quanta 3D DualBeam).

Scanning electron microscopy (SEM) images of the nanosheet film, membrane and cross sections prepared by FIB were acquired using JEOL 6700 microscope operating at 1.5 kV. Cross-section specimens were tilted to 40–48° for SEM imaging.

Xylene isomer vapor permeation measurements were carried out as reported before.[4]

Results and Discussion

Zeolite nanosheet purification by DGC

Melt compounded zeolite-polystyrene nanocomposites consist of 96% w/w polystyrene and 4% w/w MFI-nanosheets. Upon dissolution of the zeolite-polystyrene nanocomposite in toluene by sonication, MFI-nanosheets dispersed in toluene. During centrifugation of this suspension at 40,000 g for 3 h, MFI-nanosheets sedimented at the bottom of the centrifuge tube due to the difference of density between nanosheets ($\rho \sim 2.00$–2.20 g/cc), and toluene (0.87 g/cc). Since, polystyrene remains dissolved in the supernatant phase (toluene), the sediment consists of mostly MFI-nanosheets. However, the MFI-nanosheets sediment obtained after

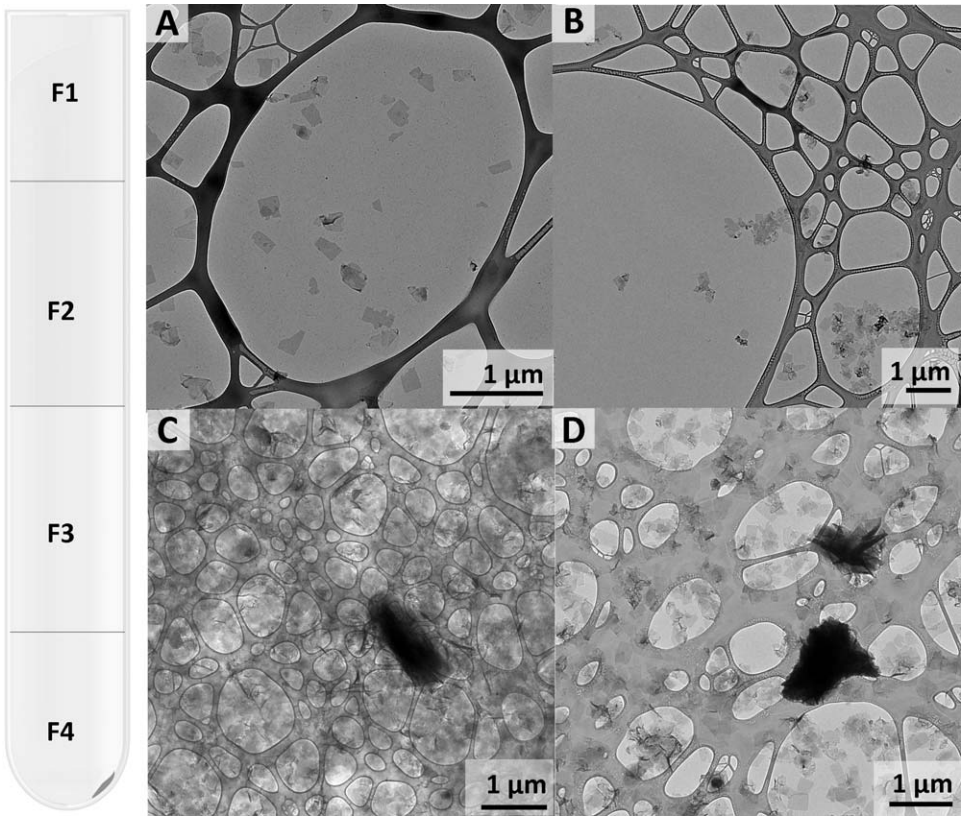

Figure 3. Left: Schematic of a centrifuge tube showing the four fractions obtained after the nonlinear density gradient centrifugation (DGC) (F1: *n*-octanol fraction; F2: chlorobenzene; F3: dichloromethane and F4: chloroform fractions). Right: the corresponding TEM images.

(A) Top (n-octanol) fraction showing MFI-nanosheets completely purified from unexfoliated particles, and (B) agglomerated MFI-nanosheets in the chlorobenzene fraction. Larger unexfoliated particles in dichloromethane (C) and chloroform (D) fractions.

discarding the supernatant is wet with toluene, and consequently polystyrene dissolved in the toluene. The amount of polystyrene can be further reduced by redispersion of the sediment in fresh toluene followed by repetition of the centrifugation process. However, despite this repeated centrifugation and redispersion washing process, it is not possible to completely eliminate polystyrene from the zeolite sediment. Figure 2A shows the image of the nanosheet sediment purified by five cycles of centrifugation and redispersion, dispersed in *n*-octanol. Polystyrene, which is insoluble in *n*-octanol, can be seen as spherical particles in the TEM image.

Instead of purification by repeated centrifugation and washing, MFI-nanosheets can be purified from polystyrene using DGC. Centrifugation of the zeolite sediment dispersed in toluene across a step density gradient of toluene/chlorobenzene enables efficient removal of polystyrene (Figure 2B). The density of polystyrene ($\rho = 1.06$ g/cc) is lower than that of chlorobenzene ($\rho = 1.10$ g/cc). Also, since chlorobenzene is a poor solvent of polystyrene, polystyrene does not diffuse in the chlorobenzene fraction during centrifugation. On the other hand, denser zeolite nanosheets ($\rho \sim 2.00$–2.20 g/cc) sediment in the chlorobenzene fraction and deposit at the bottom of the centrifuge tube (see the schematic in Figure 2C). TGA curves of the nanosheet sediments from two separate experiments indicate complete removal of polystyrene (Figure 2C). The weight loss of zeolite sediment during heat treatment to 550°C can be accounted for by the expected loss due to the removal of the organic structure directing agent (OSDA) associated with the MFI-nanosheets.[8,44] Theoretically, OSDA embedded in the straight pore channels (along the *b*-axis of nanosheets), comprises 20% of the weight of the 1.5 unit cell thick MFI-nanosheets. Extra-framework OSDA, which are loosely held on the surface of nanosheets, comprises another 21% of the weight of MFI-nanosheets, as estimated by the TGA curve in Figure S1. Some of these loosely adhered extra-framework OSDA are expected to be washed away during the DGC processing. Based on this, DGC purified nanosheets are expected to lose 20–41% of their weight in the TGA experiment. The weight loss of DGC processed nanosheets from two separate experiments reported here are well within this range (Figure 2C), indicating complete removal of polystyrene.

MFI-nanosheets purified from polystyrene using nonlinear DGC, did not disperse well in toluene, and agglomerated and sedimented within minutes. Perhaps, the presence of large amount of polystyrene in the unpurified suspension, aided the dispersion of nanosheets in toluene. Moreover, due to presence of long hydrophobic tail of OSDA on the surface of MFI-nanosheets, it is not possible to prepare a stable dispersion of nanosheets in aqueous medium. Therefore, a number of organic solvents were explored to obtain a complete dispersion of MFI-nanosheets. Among them (cyclohexane, *n*-hexane, chloroform, dichloromethane, chlorobenzene, tetrahydrofuran, ethanol, *n*-butanol, and *n*-octanol), *n*-octanol dispersed the nanosheets most effectively, and the resulting suspension was stable for many days.

Modification of the density of MFI-nanosheets by surfactant encapsulation and subsequent isopycnic centrifugation[24]

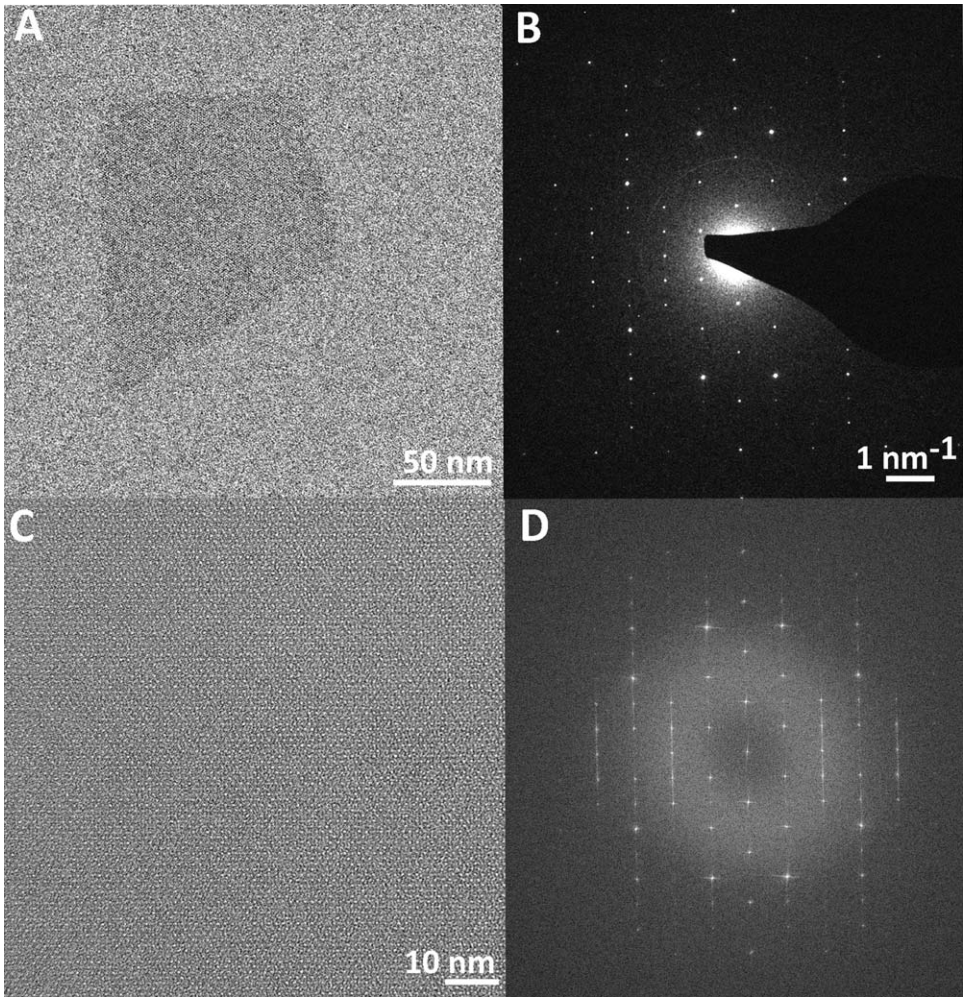

Figure 4. (A) TEM image of *b*-oriented MFI-nanosheets purified from polystyrene and unexfoliated nanosheets by DGC, (B) ED pattern from the MFI-nanosheet shown in A, (C) HRTEM image of a *b*-oriented MFI-nanosheet purified by DGC, and (D) the FFT of the HRTEM image in C.

is difficult due to the presence of the long tail OSDA on the surface of the nanosheets.[8,43,44] Instead, exfoliated nanosheets can be separated from larger unexfoliated nanosheets based on the differences in sedimentation rate, using rate-zonal centrifugation. A nonlinear density gradient created by a simple stacking of fluids with varying density has been proved effective in separating particles based on their size and shape.[34] Based on this, purification was carried out by placing nanosheet suspension in n-octanol ($\rho = 0.82$ g/cc) over density stacks created by cholorobenezene ($\rho = 1.10$ g/cc), dicholoromethane ($\rho = 1.33$ g/cc), and choloroform ($\rho = 1.48$ g/cc), followed by a mild centrifugation at 12,000 g for 30 min. Four fractions, marked by the solvent interfaces, were collected and analyzed by TEM, as shown in Figure 3. A quantitative survey on the presence of unexfoliated nanoparticles in each fraction was done by counting the number of unexfoliated particles per 5,000 exfoliated nanosheets. There were no unexfoliated particles per 5,000 exfoliated nanosheets in the top fraction (F1). Two unexfoliated particles per 5,000 nanosheets were found in the 2nd fraction from top (F2). There were a large number of unexfoliated particles in the 3rd (F3) fraction, while the 4th fraction (F4) primarily comprised of unexfoliated particles.

Figure 3A shows TEM image of F1. The presence of segregated, *b*-oriented MFI-nanosheets with uniform contrast is indicative of uniform thickness of nanosheets. Parts of the nanosheets are chipped, perhaps due to vigorous sonication of the zeolite sediments for redispersion during the purification process. The MFI-nanosheets obtained by this purification process are polydisperse in their lateral dimension (aspect-ratio). Further optimization of DGC is needed to limit the polydispersity in aspect-ratio of MFI-nanosheet for improvement in packing efficiency of the nanosheets. TEM images of MFI-nanosheets in F2, F3 and F4 are shown in Figure 3B, C, and D, respectively. MFI-nanosheets in these fractions are agglomerated, which can be attributed to the instability of nanosheets in chlorobenzene, dichloromethane and choloroform. The yield of exfoliated MFI-nanosheets in F1 is 10%, which is a twofold improvement vs. the yield of exfoliated MFI-nanosheets reported before.[4] Future work will focus on further improvement of the yield of the MFI-nanosheets purified by DGC.

Figure 4A shows a higher magnification TEM image of a MFI-nanosheet from F1. The nanosheet is *b*-oriented (i.e., with their *b*-axis along the direction of the e-beam) as it lays flat on the TEM grid due to its high-aspect-ratio ($\sim$100). The electron diffraction (ED) pattern of the nanosheet in Figure 4A is shown in Figure 4B. The presence of diffraction spots corresponding to *d*-spacing as small as 1.96 Å establishes that purified MFI-nanosheets are highly

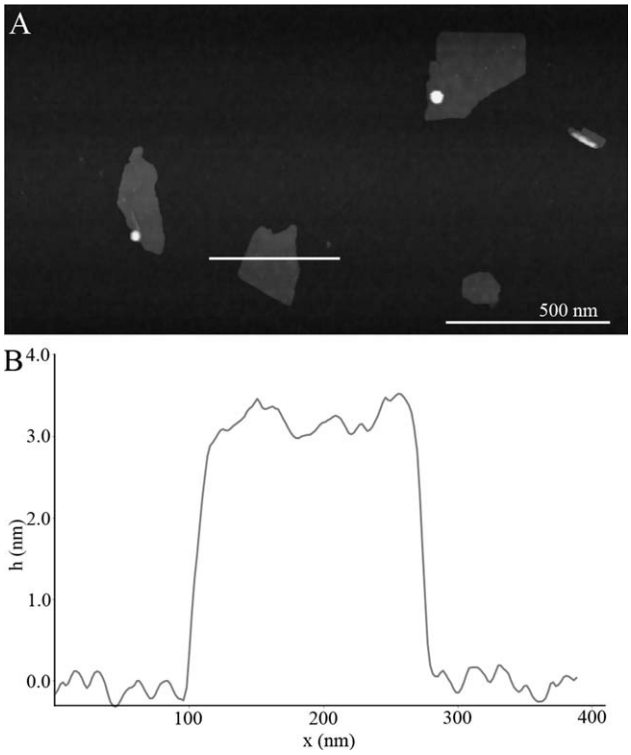

Figure 5. (A) AFM (tapping mode) topographical image of MFI-nanosheets on Si wafer, and (B) plot showing the topographical data (height vs. length) along the line scan across an MFI-nanosheet in (A).

crystalline. The ED pattern of 10 randomly chosen MFI-nanosheets was studied. All 10 nanosheets exhibited ED pattern of MFI oriented along *b*-axis, indicating absence of an amorphous phase. Figure 4C shows a high-resolution TEM (HRTEM) image of a part of a *b*-oriented MFI-nanosheet. The HRTEM image has a low contrast because MFI-nanosheets are only 3.2 nm thick.[4] The bright spots in the HRTEM images are due to the 10 member ring (MR) MFI straight pore channels running along the *b*-axis. The fast Fourier transform (FFT) of the image (Figure 4D) indicates 2.4 Å resolution, comparable to that attainable by imaging of regular zeolite crystals.

Figure 5A shows a topographical AFM image of MFI-nanosheets deposited on a silicon wafer. The nanosheets lay flat on the silicon wafer because of their high-aspect ratio. A statistical analysis of the height distribution in the AFM data yielded that the MFI-nanosheet is 3.21 ± 0.26 nm thick, corresponding to a 1.5 unit cell thickness along its *b*-axis. This along with a line scan data in Figure 5B, is consistent with the thickness of MFI-nanosheets reported before.[4]

Improved α-Alumina Support for Nanosheet Deposition

Purified nanosheets with high crystallinity are advantageous for fabrication of thin zeolite films for applications such as high-throughput membranes. However, a smooth porous support with surface roughness less than the thickness of the desired zeolite film is essential for fabrication of a compact film. The alumina support fabricated by hydraulic pressing and sintering of 400 nm α-alumina particles had a surface roughness more than 500 nm even after polishing (Figure 6A), making it extremely difficult to fabricate a sub-100-nm thick zeolite membrane without the use of an intermediate smoothening layer.[4] The high-surface roughness in this support can be attributed to the poor packing of alumina particles as they are highly agglomerated in the powder form.

To improve surface quality, supports were prepared from colloidal dispersions. Strong electrostatic repulsion between positively charged alumina particles is achieved in aqueous dispersions at pH in the 2–3 range.[48] The alumina suspension at pH 2.2 had many bubbles, which ruin the uniformity of the support surface (Figure S2A), and, hence, n-octanol was added as an antifoam agent to suppress the bubbles in the suspension.[49,50] Figure 6B shows an SEM image of the top surface of the alumina support prepared with the gypsum mold. The surface this support is much smoother than that made by powder pressing. The improved surface quality may be attributed greater degree of dispersion of the particles in suspension as compared to the bulk powder. Additionally, the open mold process may have allowed the colloidal ceramic particles to accumulate on the flat air–water interface during casting. However, a significant deposition of gypsum derived $CaSO_4.2H_2O$ on the support surface made it difficult to use this support for ultrathin zeolite film. Figure 6C shows an SEM image of the top surface of alumina support fabricated by vacuum assisted filtration. The surface roughness of this support is the lowest among the three supports due to controlled deposition and elimination of contaminants in the suspension.

Sintering of dispersion processed alumina supports at 1150°C, the temperature typically used for sintering of the

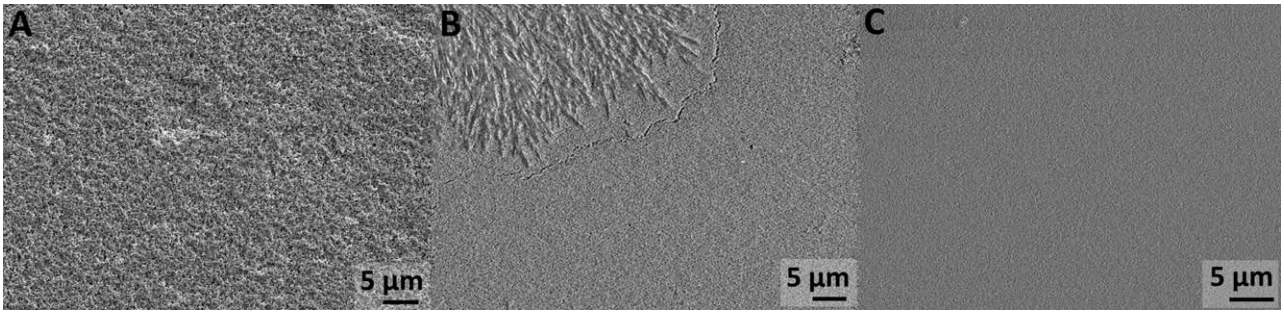

Figure 6. SEM images (top view) of the microstructure of α-alumina supports prepared by hydraulic pressing and colloidal dispersion processing.

(A) Rough surface microstructure of the support prepared by hydraulic pressing of α-alumina powder followed by sintering at 1160°C and polishing, (B) surface of support prepared by casting the alumina suspension on gypsum mold and sintered at 1050°C, and (C) smooth surface of α-alumina supports prepared by vacuum assisted filtration of alumina suspension and sintered at 1050°C.

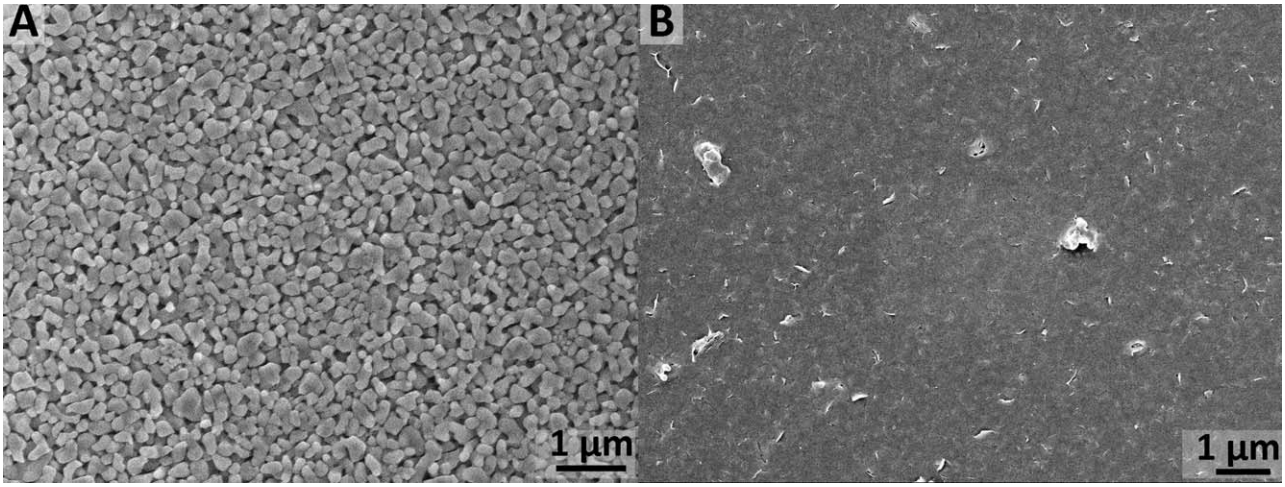

Figure 7. (A) SEM image of the surface of alumina support prepared by vacuum assisted filtration and sintered at 1050°C, and (B) SEM image of the surface of support coated with a thin film of MFI-nanosheets.

alumina disk prepared by hydraulic pressing of the alumina powder, led to partial closure of the surface pores (Figure S2B). This result can be attributed to the higher packing density of the alumina particles in the dispersion-processed disk. Reduction of sintering temperature to 1050°C led to a smooth and uniform surface microstructure, suited for the fabrication of ultrathin nanosheet films (Figure 7A).

MFI-nanosheet Film and Membrane

Fabrication of a uniform sub-100-nm thick nanosheet film on a porous support is a challenging task by traditional evaporation induced self-assembly (EISA) techniques such as dip coating or convective assembly. Surface wettability issues combined with dripping of coated films, edge effects, and capillary infiltration in porous substrates, make it challenging to control the film thickness uniformly over the entire substrate. Also, EISA requires a fairly large quantity of coating suspension in a concentration of 0.1% or above. In contrast, filtration of nanosheet suspension through a porous substrate is a simple and reproducible technique capable of producing uniform, compact and oriented films.[4] Control of film thickness can be simply achieved by adjusting the amount of suspension added for the filter coating. Also, this

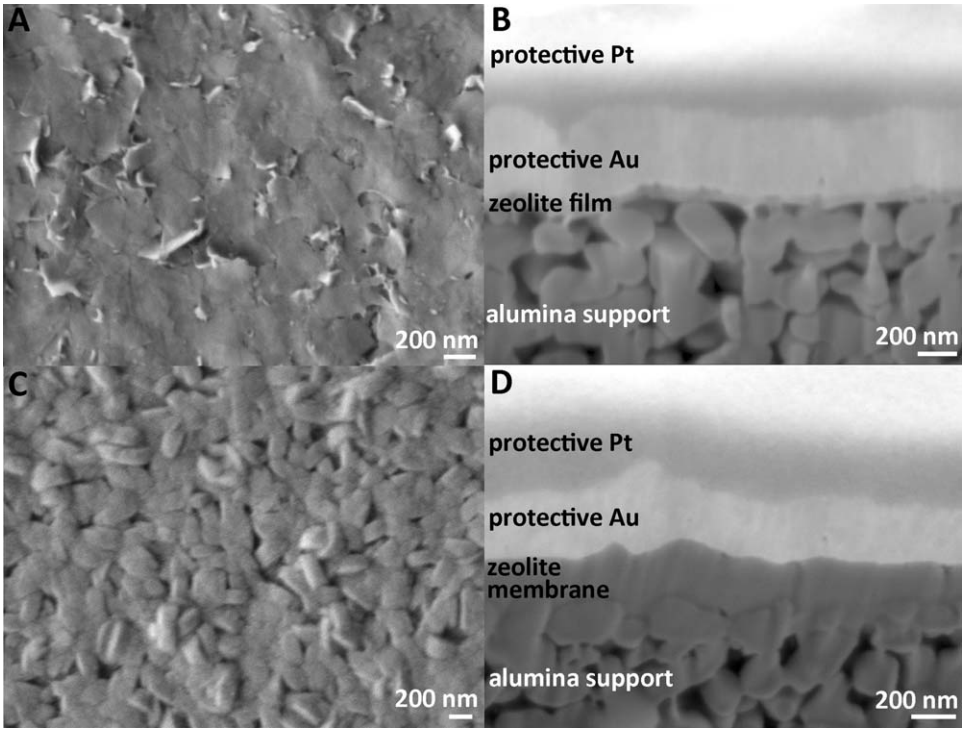

Figure 8. SEM images of the MFI-nanosheet films and their cross section prepared by FIB.

(A) Top view image of MFI-nanosheet film on the α-alumina support, (B) cross-sectional image of the film shown in A, acquired at a tilt angle of 48°, (C) top view image of membrane prepared by secondary growth of nanosheet film shown in A, and (D) cross-sectional image of the membrane shown in C, acquired at a tilt angle of 40°. The protective gold and platinum coatings are deposited to prevent beam-damage to the film/membrane surface during preparation of cross sections by FIB.

technique does not require concentrated coating suspension, thereby allowing the use of dilute nanosheet suspensions.

A thin film of MFI-nanosheets was coated on the high-quality α-alumina support by vacuum assisted filtration of the purified nanosheets suspension (Figure 7B). The coating was heat-treated at 540°C to remove the OSDA, and promote interparticle bonding by condensation of terminal silanol groups at the surface of nanosheets. Figure 8A shows a high-magnification SEM image of the top surface of the coating. MFI-nanosheets cover the entire support while orienting themselves along their *b*-axis. *b*-orientation of MFI film is advantageous for fabrication of a high-throughput membrane, as the fastest transport channel in the MFI crystal is along the b-axis.[51,52] Although the nanosheet film is compact, interparticle gaps of a few nm can be observed. These gaps could be due to the presence of a few agglomerated nanosheets in the coating suspension or curling of larger nanosheets during deposition. Future work will focus on fractionation of nanosheets based on their lateral size to further improve the packing of nanosheets in the coated film. Figure 8B shows the cross section of the nanosheet film prepared by FIB. The nanosheet film sandwiched between α-alumina support and the protective gold coating are 80 nm thick. The nanosheet coating follows the surface contour of the underlying α-alumina support because of the flexibility of high-aspect-ratio nanosheets.

Molecular sieving performance of the MFI-nanosheet film was tested by permeating an equimolar mixture of *p*-xylene and *o*-xylene through the film.[51–53] MFI nanosheets have pore openings of 0.56 nm × 0.54 nm along their *b*-axis, whereas the kinetic diameter of *p*-xylene and *o*-xylene are 0.58 nm and 0.68 nm, respectively. However, due to the presence of many interparticle gaps in the nanosheet film, separation of smaller *p*-xylene molecules did not take place, indicating a dominant contribution of flow through the larger interparticle gaps created during nanosheet coating. Mild secondary growth of this film, as per previously reported growth method,[4] led to reduction in the interparticle defects in the zeolite film. Figure 8C shows an SEM image of the top surface of the secondary-grown film after calcination. The microstructure of the film suggests twinning of zeolite nanosheets leading to growth of *a*-oriented MFI crystal. Similar twinning has been reported earlier in these growth conditions.[53] Figure 8D shows an SEM image of the cross section of the membrane prepared by FIB, indicating that the nanosheet film grew from 80 nm to 200 nm during the hydrothermal treatment. The increase in thickness of the nanosheet film is due to twinning and subsequent growth of *a*-oriented MFI crystals. Four membranes prepared by this method, separated an isomolar mixture of *p*-xylene and *o*-xylene with separation factor of 25–45, and *p*-xylene permeance of 4×10^{-7} mol/m^2-Pa-s (~375 kg/m^2-day-atm) at 150°C. The *p*-xylene permeance through the nanosheet membrane was similar to that of the alumina support.

Conclusions

These findings indicate that a nonlinear density gradient of organic solvents can be used to purify exfoliated MFI-nanosheets prepared by melt compounding of multilamellar MFI. Excessive polystyrene present in the nanosheet suspension was removed by DGC of the suspension across chlorobenzene. Rate-zonal centrifugation of nanosheets, in a multilayered density gradient, separated exfoliated nanosheets from larger unexfoliated particles. ED and HRTEM imaging of the purified MFI-nanosheets indicated that exfoliated MFI-nanosheets obtained by this process were highly crystalline. A simple filtration of purified nanosheets through improved quality porous supports led to fabrication of an 80-nm-thick MFI-nanosheet film, which upon a secondary growth to 200-nm-thick film exhibited molecular sieving capabilities for xylene isomers.

Acknowledgments

Nanosheet synthesis was supported by the Catalysis Center for Energy Innovation, an Energy Frontier Research Center funded by DOE's Office of Science, Office of Basic Energy Sciences under Award Number DESC0001004. High-quality alumina support synthesis was supported by the DOE (DE-09FE0001322), and the membrane testing by Petroleum Institute of Abu Dhabi through the ADMIRE (Abu Dhabi-Minnesota Institute for Research Excellence) partnership. Portions of this work were conducted at the University of Minnesota, Institute of Technology Characterization Facility and Nanofabrication Center, which receives partial support from the National Science Foundation through NNIN program. MT and the University of Minnesota have financial interest arising from a right to receive royalty income as described in Ref. 5. BT acknowledges financial support from Scientific and Technological Research Council of Turkey (TUBITAK, grant number BIDEP-2219). Financial support for MN from the Aragón Government, ESF, and the Spanish Ministry of Education, Culture and Sport (FPU program and MAT2010-15870) is gratefully acknowledged. MT acknowledges the generous support provided by the Amundson Chair Fund at the University of Minnesota.

Notation

Abbreviations

DGC = Density Gradient Centrifugation
OSDA = Organic Structure Directing Agent
F1 = Fraction 1
F2 = Fraction 2
F3 = Fraction 3
F4 = Fraction 4

Literature Cited

1. Amundson NR. Frontiers in Chemical Engineering: Research Needs and Opportunities. *National Research Council, National Academic Press, Washington, DC;* 1988.
2. Tsapatsis M. Toward high-throughput zeolite membranes. *Science*. 2011;334(6057):767–768.
3. Jeong HK, Nair S, Vogt T, Dickinson LC, Tsapatsis M. A highly crystalline layered silicate with three-dimensionally microporous layers. *Nature Mater*. 2003;2(1):53–58.
4. Varoon K, Zhang X, Elyassi B, et al. Dispersible exfoliated zeolite Nnanosheets and their application as a selective membrane. *Science*. 2011;334(6052):72–75.
5. Zhang XY, Liu DX, Xu DD, et al. Synthesis of self-pillared zeolite nanosheets by repetitive branching. *Science*. 2012;336(6089):1684–1687.
6. Hedlund J, Jareman F, Bons AJ, Anthonis M. A masking technique for high quality MFI membranes. *J Membr Sci*. 2003;222(1-2):163–179.
7. Lee PS, Zhang XY, Stoeger JA, et al. Sub-40 nm zeolite suspensions via disassembly of three-dimensionally ordered mesoporous-imprinted silicalite-1. *J Amer Chem Soc*. 2011;133(3):493–502.
8. Choi M, Na K, Kim J, Sakamoto Y, Terasaki O, Ryoo R. Stable single-unit-cell nanosheets of zeolite MFI as active and long-lived catalysts. *Nature*. 2009;461(7261):246–U120.

9. Pretlow TG, Pretlow TP. Separation of cells by sedimentation. In Kompala D. et al. *Cell Sep Sci Technol. ACS Symposium Series*; 1991;464:90–102.
10. Pretlow TG, Pretlow TP. Velocity sedimentation of cells. *Nature*. 1988;333(6168):97.
11. Meselson M, Stahl FW, Vinograd J. Equilibrium sedimentation of macromolecules in density gradients. *PNAS*. 1957;43(7):581–588.
12. Leif RC, Vinograd J. The distribution of buoyant density of human erythrocytes in bovine albumin solutions. *PNAS*. 1964;51:520–528.
13. Haskill JS, Moore MA. Two-dimensional cell separation: comparison of embryonic and adult haemopoietic stem cells. *Nature*. 1970;226(5248):853–854.
14. Timonen T, Saksela E. Isolation of human NK cells by density gradient centrifugation. *J Immunol Methods*. 1980;36(3-4):285–291.
15. Friedman SL, Roll FJ. Isolation and culture of hepatic lipicytes, kupffer cells, and sinusoidal endothelial-cells by density gradient centrifugation with stractan. *Anal Biochem. Feb* 1987;161(1):207–218.
16. Radajewski S, Ineson P, Parekh NR, Murrell JC. Stable-isotope probing as a tool in microbial ecology. *Nature*. 2000;403(6770):646–649.
17. Hirano T, Kobayashi R, Hirano M. Condensins, chromosome condensation protein complexes containing XCAP-C, XCAP-E and a xenopus homolog of the drosophila barren protein. *Cell*. 1997;89(4):511–521.
18. Featherstone C, Russell P. Fission yeast P107WEE1 mitotic inhibitor is a tyrosine serine kinase. *Nature*. 1991;349(6312):808–811.
19. Pertoft H. Fractionation of cells and subcellular particles with Percoll. *J Biochem Biophys Methods*. 2000;44(1-2):1–30.
20. Vauthier C, Schmidt C, Couvreur P. Measurement of the density of polymeric nanoparticulate drug carriers by isopycnic centrifugation. *J Nanopart Res*. 1999;1(3):411–418.
21. Quintanar-Guerrero D, Allemann E, Doelker E, Fessi H. Preparation and characterization of nanocapsules from preformed polymers by a new process based on emulsification-diffusion technique. *Pharma Res*. 1998;15(7):1056–1062.
22. Cardoso ALH, Neto JMM, Cardoso A, Galembeck F. Chemical heterogeneity in poly styrene-*co*-(butyl methacrylate) copolymer latexes prepared using different monomer addition modes. A study by isopycnic centrifugation in density gradient. *Colloid Polym Sci*. 1997;275(3):244–253.
23. Neto JMM, Cardoso ALH, Testa AP, Galembeck F. Heterogeneity in polymer latices-detection by zonal centrifugation. *Langmuir*. 1994;10(7):2095–2099.
24. Arnold MS, Green AA, Hulvat JF, Stupp SI, Hersam MC. Sorting carbon nanotubes by electronic structure using density differentiation. *Nature Nanotechnol*. 2006;1(1):60–65.
25. Yanagi K, Miyata Y, Kataura H. Optical and conductive characteristics of metallic single-wall carbon nanotubes with three basic colors; Cyan, magenta, and yellow. *Appl Phys Express*. 2008;1:034003-1–034003-3.
26. Ghosh S, Bachilo SM, Weisman RB. Advanced sorting of single-walled carbon nanotubes by nonlinear density-gradient ultracentrifugation. *Nature Nanotechnol*. 2010;5(6):443–450.
27. Niyogi S, Densmore CG, Doom SK. Electrolyte tuning of surfactant interfacial behavior for enhanced density-based separations of single-walled carbon nanotubes. *J Amer Chem Soc*. 2009;131(3):1144–1153.
28. Yanagi K, Iitsuka T, Fujii S, Kataura H. Separations of metallic and semiconducting carbon nanotubes by using sucrose as a gradient medium. *J Phys Chem C*. 2008;112(48):18889–18894.
29. Green AA, Hersam MC. Processing and properties of highly enriched double-wall carbon nanotubes. *Nature Nanotechnol*. 2009;4(1):64–70.
30. Green AA, Hersam MC. Properties and application of double-walled carbon nanotubes sorted by outer-wall electronic type. *Acs Nano*. 2011;5(2):1459–1467.
31. Fagan JA, Becker ML, Chun J, Hobbie EK. Length fractionation of carbon nanotubes using centrifugation. *Adv Mater*. 2008;20(9):1609–+.
32. Lu Q, Keskar G, Ciocan R, et al. Determination of carbon nanotube density by gradient sedimentation. *J Phys Chem B*. 2006;110(48):24371–24376.
33. Zhang MF, Yamaguchi T, Iijima S, Yudasaka M. Individual single-wall carbon nanohorns separated from aggregates. *J Phys Chem C*. 2009;113(26):11184–11186.
34. Sun XM, Tabakman SM, Seo WS, et al. Separation of nanoparticles in a density gradient: FeCo@C and gold nanocrystals. *Angew Chem Intl*. 2009;48(5):939–942.
35. Tyler TP, Henry AI, Van Duyne RP, Hersam MC. Improved monodispersity of plasmonic nanoantennas via centrifugal processing. *J Phys Chem Lett*. 2011;2(3):218–222.
36. Mastronardi ML, Hennrich F, Henderson EJ, et al. Preparation of monodisperse silicon nanocrystals using density gradient ultracentrifugation. *J Amer Chem Soc*. 2011;133(31):11928–11931.
37. Green AA, Hersam MC. Solution phase production of graphene with controlled thickness via density differentiation. *Nano Lett*. 2009;9(12):4031–4036.
38. Sun XM, Luo DC, Liu JF, Evans DG. Monodisperse chemically modified graphene obtained by density gradient ultracentrifugal rate separation. *ACS Nano*. 2010;4(6):3381–3389.
39. Woolson EA, Axley JH. Clay separation and identification by a density gradient procedure. *Soil Sci Soc Amer J*. 1969;33(1):46–48.
40. Jaynes WF, Bigham JM. Concentration of iron-oxides from soil clays by density gradient centrifugation. *Soil Sci Soc Amer J*. 1986;50(6):1633–1639.
41. Bai L, Ma XJ, Liu JF, Sun XM, Zhao DY, Evans DG. Rapid separation and purification of nanoparticles in organic density gradients. *J Amer Chem Soc*. 2010;132(7):2333–2337.
42. Ma XJ, Kuang Y, Bai L, et al. Experimental and mathematical modeling studies of the separation of zinc blende and wurtzite phases of cdS nanorods by density gradient ultracentrifugation. *Acs Nano*. 2011;5(4):3242–3249.
43. Na K, Choi M, Park W, Sakamoto Y, Terasaki O, Ryoo R. Pillared MFI zeolite nanosheets of a single-unit-cell thickness. *J Amer Chem Soc*. 2010;132(12):4169–4177.
44. Corma A. Catalysts made thinner. *Nature*. 2009;461(7261):182–183.
45. Maheshwari S, Jordan E, Kumar S, et al. Layer structure preservation during swelling, pillaring, and exfoliation of a zeolite precursor. *J Amer Chem Soc*. 2008;130(4):1507–1516.
46. Choi J, Ghosh S, King L, Tsapatsis M. MFI zeolite membranes from a- and randomly oriented monolayers. *Adsorption*. 2006;12(5-6):339–360.
47. Nagahara LA, Hashimoto K, Fujishima A, Snowdenlfft D, Price PB. Mica etch pits as a height calibration source for atomic-force microscopy. *J Vac Sci Technol B*. 1994;12(3):1694–1697.
48. Cesarano J, Aksay IA. Processing of highly concentrated aqueous alpha-alumina suspensions stabilized with poly-electrolytes. *J Am Ceram Soc*. 1988;71(12):1062–1067.
49. Luo LH, Tok AIY, Boey FYC. Aqueous tape casting of 10 mol %-Gd2O3-doped CeO2 nano-particles. *Mater Sci Eng A*. 2006;429 (1-2):266–271.
50. Zhang D, Su B, Button TW. Microfabrication of three-dimensional, free-standing ceramic MEMS components by soft moulding. *Adv Eng Mater*. 2003;5(12):924–927.
51. Lai ZP, Bonilla G, Diaz I, et al. Microstructural optimization of a zeolite membrane for organic vapor separation. *Science*. 2003;300(5618):456–460.
52. Tung CTP, Kim HS, Yoon KB. Growth of uniformly oriented silica MFI and BEA zeolite films on substrates. *Science*. 2011;334(6062):1533–1538.
53. Lai ZP, Tsapatsis M, Nicolich JR. Siliceous ZSM-5 membranes by secondary growth of b-oriented seed layers. *Adv Funct Mater*. 2004;14(7):716–729.

Manuscript received Dec. 20, 2012, and revision received Feb. 11, 2013.